DENTAL MATERIALS 35 (2019) 953–962

Available online at www.sciencedirect.com

ScienceDirect

journal homepage: www.intl.elsevierhealth.com/journals/dema

Size or hierarchical dependence of the elastic modulus of three ceramic-composite CAD/CAM materials

R.A. Al-Shatti[a], G.H. Dashti[a], S. Philip[a], S. Michael[a], M.V. Swain[a,b,c,*]

[a] Faculty of Dentistry, Health Science Center, University of Kuwait, Kuwait
[b] Biomaterials and Biomechanics, Engineering, Don State Technical University, Rostov on Don, Russia
[c] AMME, The University of Sydney, Sydney Australia

ARTICLE INFO

Article history:
Received 19 October 2018
Received in revised form
18 February 2019
Accepted 27 March 2019

Keywords:
CAD/CAM
Ceramic resin composites
Elastic modulus
Hierarchical structure
Atomic force microscopy
Nano-indentation

ABSTRACT

Objective. To measure the elastic modulus of three ceramic-composite CAD/CAM materials at three different microstructural dimensions: macro, micro, and nano.

Methods. Three novel ceramic-composite CAD/CAM materials (Enamic, Lava Ultimate, and Cerasmart) were investigated. Rectangular cross-sections $10 \times 5.7 \times 1$ mm^3 ($n = 30$) were cut from standard sized milling blocks of each material prior to polishing. Specimens were macro-tested using three-point bending and with a dynamic mechanical analyzer (DMA), micro-tested using a nano-indentation system, and finally at the nano-level with an atomic force microscope (AFM). Data were analyzed with 1-way ANOVA ($\alpha = 0.05$).

Results. At the macro level Enamic showed the highest elastic modulus, followed by Lava Ultimate and Cerasmart respectively ($p < 0.001$). Measurements at the micro and nano level resulted in bimodal distributions of the elastic modulus values associated with the various phases present with values higher and lower than measured at the macro level. Only at the nano-level were the various phases of Cerasmart able to be distinguished.

Conclusions. The tested materials showed different elastic modulus at the different size or hierarchical levels that enabled comparison with the hierarchical values of enamel.

Significance. Studying the mechanical properties of these novel materials at different size or hierarchical scales can help to understand their potential clinical performance, such as structural durability and opposing tooth wear and lead to more biomimetic like dental restorative materials.

1. Introduction

CAD/CAM technology has become increasingly popular during the past 3 decades as it simplifies fabrication of dental restorations and reduces cost [1,2]. Ceramics provide high esthetics, biocompatibility and durability outcomes in the oral cavity [3,4]. However, they are brittle and susceptible to fracture [5,6]. Composites are easier to handle and repair but have high wear and reduced biocompatibility. As a consequence, polymer ceramic composite systems, following their widespread usage in chairside restorative applications, have become a new entrant to the CAD/CAM materials palette. These materials vary as to their strategies of production from polymer-infiltrated-ceramic network materials (PICNs)

* Corresponding author.
E-mail address: michael.swain@sydney.edu.au (M.V. Swain).
https://doi.org/10.1016/j.dental.2019.03.012

to near classical resin composite systems in order to overcome the disadvantages of both materials [7]. The intent of these materials are to combine the positive characteristics of both composite and ceramic in an attempt to achieve a tooth like structure and matching physical properties with less abrasiveness to the opposing dentition.

The bulk mechanical properties of these three materials of choice have been previously explored [6–10]. Recently Mainjot et al. reviewed the properties of PICNs as well as ceramic-resin composite systems and showed the latter exhibited significantly higher flexural strength and modulus of resilience than chairside composites while a number of experimental PICN systems had strengths comparable to advanced glass-ceramic systems [7]. Ceramic-resin composites due to their lower modulus exhibit greater elastic deflection before failure. On the other hand, PICNs typically exhibited mechanical behavior, especially hardness (H) and modulus (E) between human dentine and enamel while ceramic filled resin composites have values closer to dentine [11–16].

Our approach with these materials is to study the elastic modulus at different sizes or dimensional ranges, generally termed hierarchical levels for biological tissues such as enamel, which has significant clinical implications. For example, while a low E modulus in-lay or crown material may readily accommodate the flexure of a cusp under load the differential deformation at the margin may lead to interface debonding resulting in microleakage and subsequent failure coupled with susceptibility to recurrent caries [16]. It is also established that ceramic-composite CAD/CAM materials have a more favorable wear pattern in comparison to other ceramics [17]. According to Stawarczyk et al., the highest overall wear to the opposing enamel surface of the 3 materials was seen for Vita Enamic; whereas, Lava Ultimate showed the highest wear of the restoration itself [18]. However, when comparing opposing tooth wear created by these materials with that resulting from enamel, it was found that they behave similarly or better with respect to two-body wear [17]. This shows a significant biological consideration in saving healthy tissues and preventing functional shifts affecting the stability of the occlusion.

In this paper the emphasis is placed on quantifying the elastic properties of the bulk (macro) as well as at the micro and nano level. Similar observations in enamel have led to an appreciation of the hierarchical properties of calcified biological tissues and with the aim to mimic such structures in dental restorative systems. Our hypothesis is that the E modulus of the samples will depend upon specimen size.

2. Materials and methods

2.1. Materials and specimen preparation

Three different ceramic-composite CAD/CAM materials were investigated (Table 1), namely Enamic (Vita Zahnfabrik), Cerasmart (GC Dental Products) and Lava Ultimate (3 M).

Standard sized milling blocks of each material were cut using a water-cooled diamond saw (Struers, Accutom-10) to obtain 10 rectangular cross-sections per material (n = 30) with dimensions approximately ($12 \times 6 \times 1\,mm^3$). For the micro and nano tests, the slices were mounted in resin (EpoFix Resin, Struers) for easier handling and testing. The latter specimens were subsequently ground and polished with 220 through 1000 grit SiC papers under water irrigation, followed by 6 μm and 1 μm diamond suspension. Initially all specimens were examined in an optical microscope (ZEISS, Axio Imager. M2m).

2.2. Macro level tests

Testing was performed in three-point-bending using monotonic loading to fracture and with a dynamic mechanical analyzer (DMA), which uses sinusoidal loading. The DMA enabled not only the E modulus but also the tan delta or energy loss during flexural cycling to be measured.

2.2.1. Three-point bending (Instron)

Machined bars ($12 \times 6 \times 1\,mm^3$) were tested in air at laboratory temperature, using a universal testing machine (Tecton ElectroPlus E3000, Instron UK) with a calibrated 1000 N load cell, on a 10 mm span at a loading rate of 0.5 mm/min. The force-displacement curve enabled the flexural strength as well as the stress-strain response and E modulus to be determined using the Instron Bluehill software. The elastic modulus was calculated from the measured beam deflection using the following formula [19]:

$$E = \frac{FL^3}{48\,\delta I}$$

where E is the elastic modulus, F is force, L is the length of beam, δ is the deflection of the beam and I is the moment of inertia of the beam, namely:

$$I = \frac{bh^3}{12}$$

where h is the thickness or dimension in the plane of bending, i.e. in the axis in which the bending moment is applied, and b is the width of the specimen, i.e. in the orthogonal direction.

2. 2. 2. Three-point bend flexural response (DMA)

Tests were conducted using a DMA (NETZSCH DMA 242, Germany) instrument on samples (3 of each) of dimensions previously defined for the Instron tests. The temperature range was from 27 °C to 180 °C at a heating rate of 3 °C/min, frequency of 1 Hz and maximum dynamic force of 1 N. As a sinusoidal force was applied, from the resultant displacement in phase with the force the storage modulus was obtained while from the out of phase component, the loss modulus was determined. The ratio of the loss to the storage modulus is termed tan δ.

2.3. Micro level test

2.3.1. Nanoindentation

Nanoindenter tests were performed in air using a calibrated Berkovich diamond tip with a Hysitron Ubi700 (Minneapolis, MN, USA) nanoindenter. On the basis of the area function curve the indenter tip radius was estimated as approximately 90 nm. The resulting force-displacement curve is used to determine elastic modulus (E) and hardness (H) [20]. The contact elastic modulus E^* is determined from the slope of the

Table 1 – Details of the materials investigated in this study.

Material		Manufacturer	Composition
Polymer infiltrated ceramic network (PICN)	Vita Enamic	VITA Zahnfabrik, Bad Säckingen, Germany	Polymer-infiltrated-feldspatic ceramic-network material (UDMA, TEGDMA) with 86 wt% ceramic and 14 wt% polymer part
Resin composite	Lava Ultimate	3 M ESPE, Seefeld, Germany	Composite resin material (BisGMA, UDMA, BisEMA, TEGDMA) with 80 wt% silica and zirconia nanoparticles and nanoclusters with 20 wt% highly cross linked polymer matrix
	Cerasmart	GC Dental Products Europe, Leuven, Belgium	Composite resin material (BisMEPP, UDMA, DMA) 71% silica and barium glass nanoparticles

BisGMA: bisphenol A diglycidylether dimethacrylate; UDMA: urethane dimethacrylate; BisEMA: ethoxylated bisphenol A dimethacrylate; TEGDMA: triethylene glycol dimethacrylate; BisMEPP: bisphenol A ethoxylate dimethacrylate.

unloading curve, S, and the area of contact at maximum load A_c and is given by the expression [20]:

$$E^* = \frac{\sqrt{\pi}\,S}{2\sqrt{A_c}}$$

Placement of 10–20 indentations per material was done using the indenter tip scanning facilities of the instrument to visualize the microstructure. The location of the indentation points on the specimens was made manually by choosing specific sites on images of the samples generated.

As the investigated materials have mainly two distinct phases, ceramic or pre-reacted composite phase and polymer phase, initially tests were conducted over a load that ranged from 1 to 5 mN on the various phases before limiting the load in order to achieve comparable depths of penetration in the different phases. The loads used were 5 mN on the Enamic ceramic phase and 1 mN on the polymer phase while for Lava Ultimate all tests were done at 2 mN. For all the materials the inbuilt contact scanner was used to identify the locations for indentations on the various phases. However, for the Cerasmart a 4 by 4 array at 5 μm spacing at 2 mN was used as it was not possible to identify the respective phases using the contact scanner of the instrument. A hold period of 10 s at max load was included in the force-displacement data acquisition. As for the polymer, the available area for indentation was variable and generally very limited as the ceramic or pre-reacted composite phase is the dominant component in these composite systems. While we set the position of the indenter directly at the polymer phase, the machine may have drifted slightly so that contact may have occurred with the polymer-ceramic interface. In some instances, upon inspection of the impression sites post-indentation the force-displacement curves were deemed unacceptable as the contact area straddled the polymer-ceramic (pre-reacted composite) boundary. Values for *H* and *E* were generated automatically from the software using the force-displacement graphs based on the Oliver Pharr relationship [20].

2.4. *Nano level test*

2.4.1. *Atomic force microscope (AFM)*

AFM can provide high-resolution images and three-dimensional representation of the sample. The cantilevers in the AFM system were fabricated from silicon with an integrated sharp tip [21]. The tip–sample interaction affects the motion and/or the bending of the cantilever and is related to sample stiffness. Contact AFM mode was used to determine the E modulus at the nano level in which specific analysis options have to be chosen including selection of tip radius, as well as tip geometry; sphere, punch, or cone. A punch shaped tip with radius of 8 nm was selected, based upon the AFM tip supplier's documentation (silicon AC 160TS-R3, Olympus Japan).

Scans of the polished surfaces were conducted using an AFM (MFP-3D, Asylum, Oxford Scientific, UK) configured as a bimodal nanomechanical force microscope over different areas, including 20×20, 10×10, 5×5 and 2×2 μm. The resolution of the AFM was set to capture 256 data points per scan, irrespective of the scan range resulting in 65,536 data points per scanned area and at each data point values for the elastic modulus were determined. With the 2×2 μm scanned image the spacing between successive measurements of elastic modulus and topography is approximately 8 nm A major issue with the AFM method for determination of elastic modulus is that there is no standard process for tip calibration and the tip geometry changes during the course of multiple scans because of wear. In the results section we describe the calibration procedure used to determine the E modulus.

2.5. *Statistical analysis*

Data were analyzed using the Statistical Package for the Social Science (SPSS) software, version 24, IBM. Firstly, descriptive statistics, such as means and standard deviation, were computed for each property. One-way ANOVA was used to compare between the means of the three materials for the tests done in each dimension. A p-value less than 0.05 was considered statistically significant.

3. Results

3.1. *Macro results*

3.1.1. *Three-point bending (Instron)*

Typical force-displacement curves generated for the three materials are shown in Fig. 1. The Enamic material exhibited a linear loading response to fracture while the Lava Ultimate and Cerasmart material showed breakage at a higher load along with less steep and non-linear responses especially for Cerasmart. The values of the fracture strength and E modulus were determined using Instron Bluehill software. The results

Table 2 – Three-point bend (3PB) and Dynamic mechanical analyzer (DMA) comparisons of E modulus.

Material	Elastic modulus (GPa) (mean ± SD)	Maximum flexure stress (MPa) (mean ± SD)	DMA Elastic Modulus (GPa) (mean ± SD)	DMA Tan delta (mean ± SD)
Vita Enamic	31.43 ± 2.08	128.16 ± 11.04	36.12 ± 4.66	0.03 ± 0.001
Lava Ultimate	13.63 ± 2.15	163.83 ± 16.03	14.9 ± 1.09	0.05 ± 0.004
Cerasmart	9.92 ± 0.13	160.36 ± 35.2	8.76 ± 1.07	0.06 ± 0.003
Significance level	$p < 0.001$		$p < 0.001$	

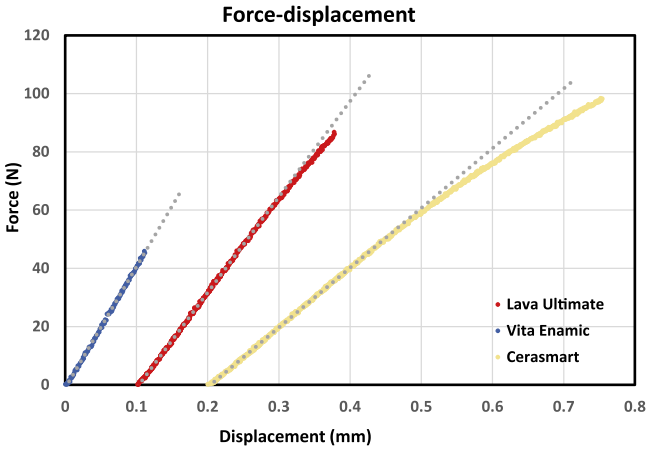

Fig. 1 – Typical force-displacement curves generated during 3 point bending of macro samples of the three CAD/CAM materials. The force-displacement curves have been offset and a linear fit to the initial loading response has been extrapolated to assist with showing the non-linear response of the Lava Ultimate and Cerasmart materials.

for the three materials are listed in (Table 2). Enamic has the highest elastic modulus, followed by Lava Ultimate and then Cerasmart. One-way ANOVA revealed a significant difference between the means ($p < 0.001$). The volume of the material tested is the size of the beam and as such is $10 \times 5.67 \times 1.03$ mm^3, 58.4 mm^3 on average.

3.1.2. *Three-point bend flexural response (DMA)*

The DMA results for the three materials as a function of temperature from 27 to 180 °C are shown in Fig. 2. These plots show both elastic modulus and tan delta values. Note that there is a reduction in elastic modulus with increasing temperature, while for tan δ Lava Ultimate and Cerasmart show a substantial increase with temperature. The tan δ values scale with the volume fraction of the polymer phases for the three materials. Table 2 also summarizes the DMA results in the temperature range from 27 to 55 °C. Based on Moore and his colleagues, the majority of the time, intra oral temperatures throughout the day range between 33 and 37 °C with maxima up to 55 °C [23,24]. The results of one-way ANOVA revealed that the material factor had a significant effect on the elastic modulus and tan δ ($p < 0.001$) of the tested specimens. Similarly, as for the Instron tests, Enamic showed the highest elastic modulus, followed by Lava Ultimate and Cerasmart respectively. Comparison of the Instron and DMA measured values of the elastic modulus for the three materials, Table 2, shows that the values were very comparable using the two approaches.

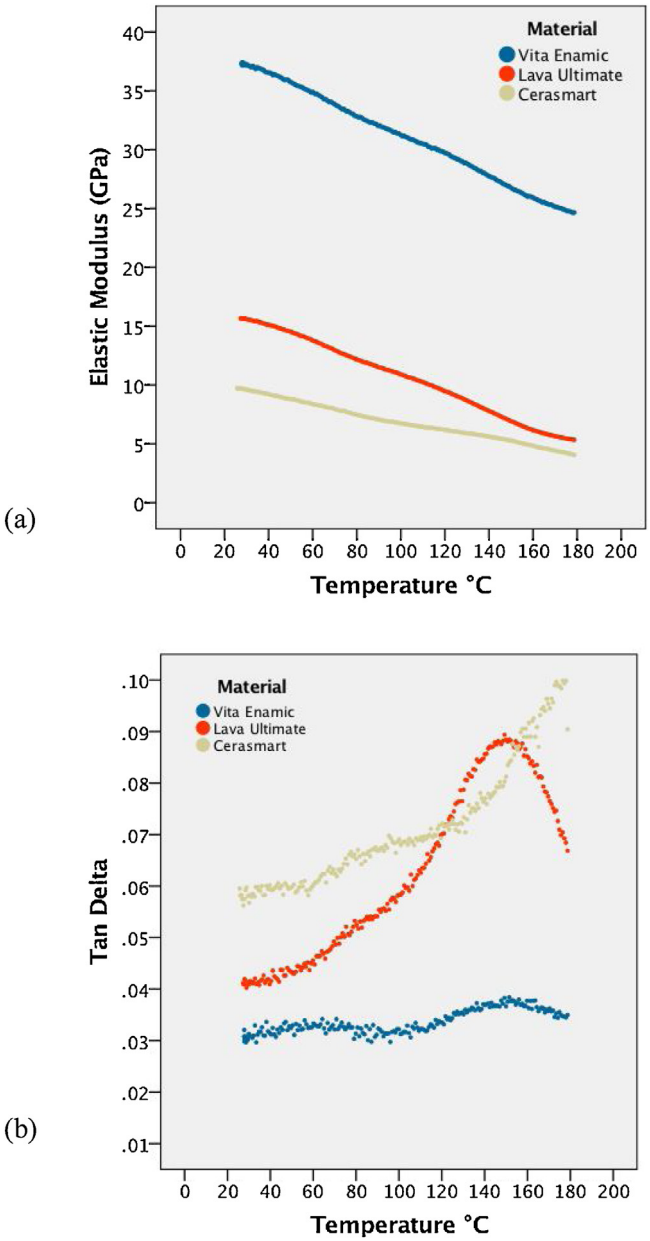

Fig. 2 – Dynamic mechanical analysis data from room temperature to 180 °C showing the variation of the storage E modulus and tan delta.

3.2. *Micro level results*

3.2.1. *Nanoindentation*

Observations of the nano-indentation tests for the three materials are shown in Fig. 3. There are two sets of data for the

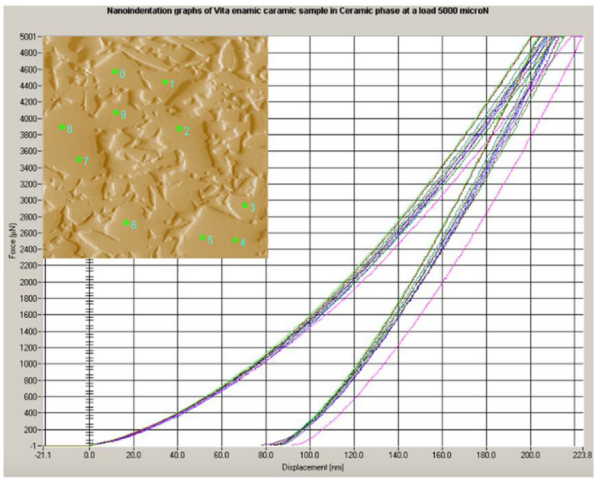

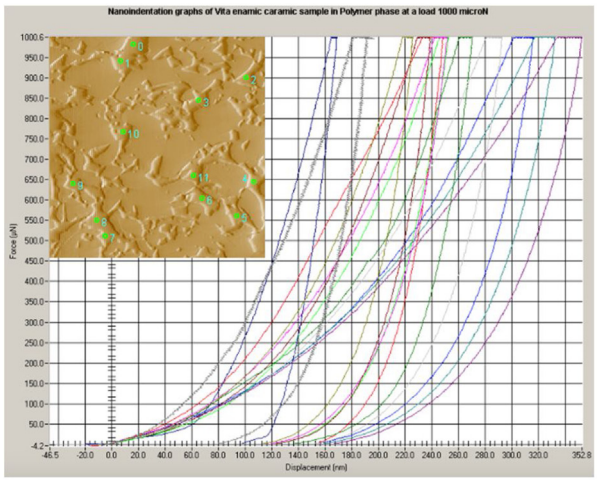

a)

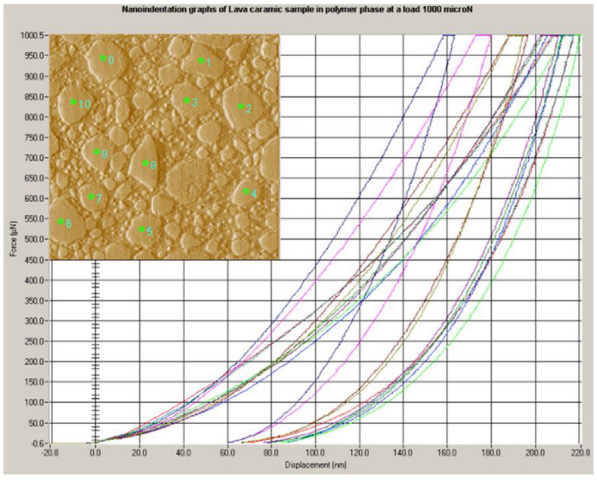

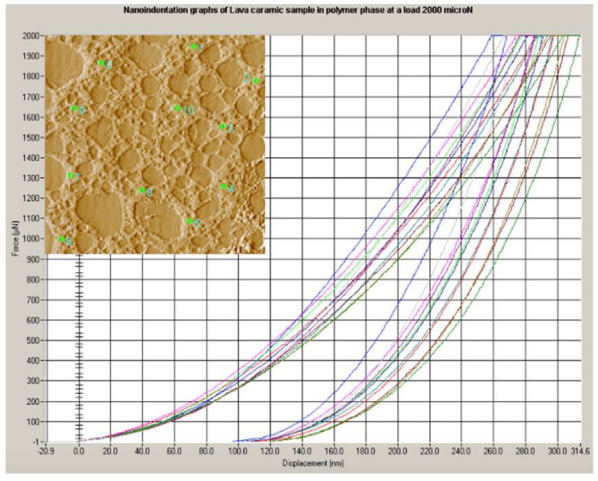

b)

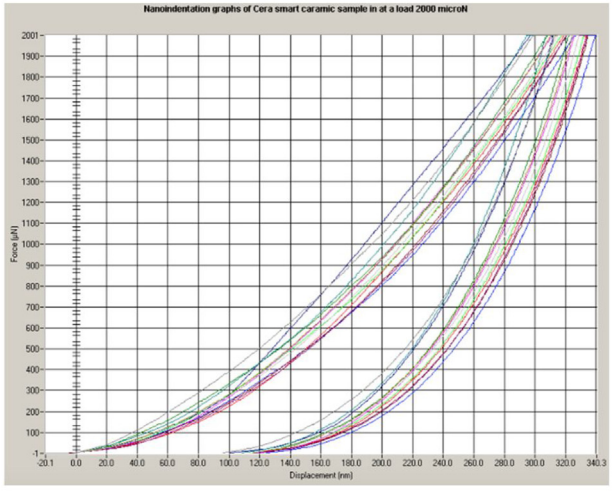

c)

Fig. 3 – Nanoindentation force-displacement curves for the three materials along with inserts (30 by 30 μm) showing the locations of the indentations on the different phases. No insert has been included with the Cerasmart material as it was not possible to identify the microstructural features with the nanoindenter AFM system.

Table 3 – Comparison of Nanoindentation and Atomic Force Microscope E modulus values.

Material		Number of tests	AFM Elastic Modulus (GPa) (mean ± SD)	NI: Elastic modulus (GPa) (mean ± SD)	NI: Hardness (GPa) (mean ± SD)
Vita Enamic	Ceramic phase	9	56.6 ± 5.7	56.81 ± 3.28	6.9 ± 0.33
	Polymer phase	12	16.87 ± 3.51	17.56 ± 7.58	0.65 ± 0.28
Lava Ultimate	Pre-reacted polymer	10	22.9 ± 2.48	25.4 ± 4.49	3.02 ± 0.74
	Polymer matrix	11	11.63 ± 1.83	17.29 ± 2.43	1.12 ± 0.26
Cerasmart	Pre-reacted particles	12	16.3 ± 1.51	13.82 ± 0.66	0.94 ± 0.67
	Polymer matrix	12	10.34 ± 2.25		
Significance level			$p < 0.05$	$p < 0.05$	$p < 0.05$

Enamic and Lava Ultimate materials as it was possible to identify the different phases and indent them separately while for the Cerasmart this was not possible as the area of contact even at 2 mN, covered multiple individual particles within the composite. The reproducibility of the force-displacement curves was excellent in the case of the ceramic phase of Enamic, for the tests on Cerasmart and to a lesser degree for the polymer phase of Enamic and the matrix polymer phase of Lava Ultimate. The results for E and H of the various phases are listed in Table 3. One-way ANOVA showed significant differences between the materials for both E and H ($p < 0.001$). In consideration of the microstructure of Enamic and Lava Ultimate, the mean E and H obtained for the ceramic and polymer phases were found to be statistically significant within each material ($p < 0.05$).

3.3. *Nano-level results: AFM*

Maps of the elastic modulus of the $2 \times 2\,\mu$m scans for the different materials are shown in Fig. 4. The maps bear a strong resemblance to the microstructure seen in the nanoindenter scans shown as the inserts in Fig. 3. However, the results for Cerasmart reveal the presence of a stiffer phase within a polymeric matrix. Initially for all these plots, the contact conditions were assumed to be close to what the supplier of the AFM tips (Asylum, AC160TS-R3) stated, namely silicon tips 8 nm radius and punch shape and therefore the associated contact area was $\tilde{2}00nm^2$. For all tests our approach to critically determine the E modulus was to utilize all the data points to determine an effective average contact modulus $\hat{E}^*$ for the flat tip radius. This was done by averaging all the weighted values of the histogram and comparing it with the expected E^* for a silicon indenter in contact with a material of the E modulus determined using the 3PB data for the bulk samples. It was found that the ratio between the expected E^* value and that determined using the flat punch geometry with 8 nm radius ($\hat{E}^*$) scaled linearly with the bulk E modulus of the material. This ratio, which is directly related to the ratio of the assumed to actual indenter contact radius, was highest for Enamic (3.194), intermediate for Lava Ultimate (1.794) and least for Cerasmart (1.508). The implication is that the tip is probably not flat but parabolic and that the penetration depth (and associated area of contact) scales with the E modulus of the area of contact. The resultant linear expression linking the ratio of AFM $\hat{E}^*$ modulus with bulk equivalent E^* modulus was used to re determine the E values and generate corrected histograms for the 3 materials. Plots of the AFM images and corrected histograms are shown in Fig. 4. For all materials there are bimodal distributions of the E modulus values indicative of the polymer, ceramic or pre-reacted resin components present. For Enamic the higher E ceramic peak is much more intense than the lower polymer peak (peak intensity ratio 2.18), for Lava Ultimate the pre-reacted and matrix polymeric peaks are almost comparable (ratio 1.39) while for the Cerasmart the polymer component is far more dominant than the secondary stiffer material (ratio 3.25). The scatter associated with the histograms was estimated assuming that the peaks had Gaussian distributions and one standard deviation occurs at 68% of the peak values. The area under the peaks is considered to reflect the volume fractions of the specific components.

Surprisingly, the scanned surface of Cerasmart shown in (Fig. 4c) clearly identifies the sub-micron components present in this material. The image generated from the elastic modulus map values clearly indicates that this material has two very different components. The relative low values of the stiffer pre-reacted phase are most likely associated with the small size of these presumably pre-reacted ceramic-resin particles, which are embedded in the polymer matrix.

4. Discussion

4.1. *Macro level*

4.1.1. *Three-point bending test (Instron)*

The force-displacement curves (Fig. 1) and resultant values of the elastic modulus and strength in Table 1 show an almost inverse relationship between strength and elastic modulus. For Enamic, the force-displacement curve and associated stress-strain curve are linear to fracture, indicative of a brittle material. Lava Ultimate and Cerasmart showed slight curvature of the force-displacement and associated stress-strain curves. The latter response indicates that Lava Ultimate and Cerasmart undergo non-linear or plastic-like deformation prior to fracture. In terms of flexural strength, the results are slightly lower for all three materials than some previous reports [11,13]. The E modulus values are close to recently reported values of the various materials [10,11].

4.1.2. *Three-point bend flexural response (DMA)*

The elastic modulus and tan δ results shown for the 3 materials in Fig. 2 indicate that there is a gradual reduction in elastic modulus with temperature. However, over the temperature range in the oral cavity 27–55 °C, there is only a modest

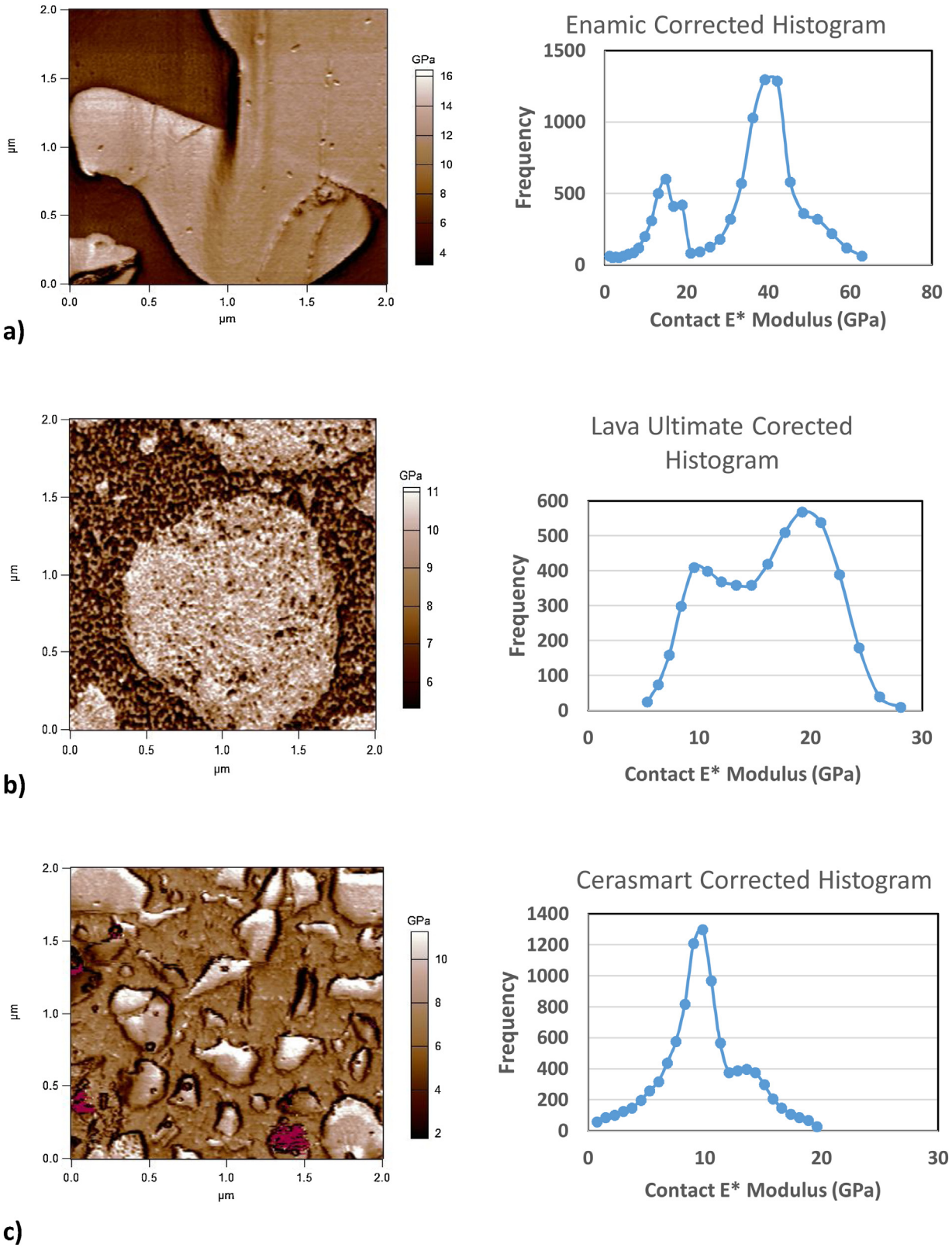

Fig. 4 – Atomic force microscopy images of the E modulus of the three materials generated with 2 by 2 µm scans, along with a scale bar of the E modulus assuming an 8 nm radius flat punch tip, for; (a) Enamic, (b) Lava Ultimate and (c) Cerasmart. Adjacent to the image scans are plots of the corrected E modulus generated from the frequency distributions from all the contact points (65,536) associated with the AFM scan.

decrease in E and the values in this range were averaged to enable comparison with Instron derived results and found to be similar. The tan δ results show the opposite effect to the elastic modulus, in that, apart from Enamic, they increase with temperature suggesting that energy dissipation processes are becoming more influential. The Enamic values of tan δ are similar to those reported by Behin et al. [25]. There are clear minor maxima at 60 °C and 150 °C for Enamic, 80 °C and major peak (Tg or glass transition temperature) at 150 °C for Lava Ultimate, while Cerasmart shows a minor peak at 80–90 °C and then continues to rise with a major peak and presumably Tg above 180 °C, the highest temperature measured in this study. The DMA values generated show similarity with results by Behin et al. [25] for BisGMA and other dental resins in high pressure/high temperature (HP/HT) matrices that suggested these polymers had an increased crosslink density. In addition, these authors found that the higher polymerization temperature or the lack of initiator had a beneficial effect, which is a reduction of the viscous properties [25]. Furthermore, Ruse and Sadoun found that polymerization under HP/HT led to noticeable changes in surface morphology, which was revealed with AFM characterization [5]. Shah et al. [26] have recently explored the DMA response of a range of Bis-GMA polymers and have identified peaks at 60 °C and 150 °C, which are similar to the results for the current Enamic and more so for Lava Ultimate. The lower temperature peak is associated with the partially polymerized oligomer whereas the higher temperature Tg peak is for the more highly-densified and cross-linked structure [26]. The Cerasmart shows a different behavior with a higher apparent Tg which may be related to the different composition of the resin phase.

4.2. *Micro level*

4.2.1. *Nano-indentation*

The difference between the three materials in terms of the elastic modulus and hardness at this level is clear. Additionally, it was noted that the elastic modulus and hardness differences are also statistically significant ($p < 0.05$) when comparing the ceramic (or pre-reacted ceramic-resin phases) and polymer phases for both Enamic and Lava Ultimate. Due to size of the two phases in Cerasmart, the same comparison was not possible for this material. The highest elastic modulus and hardness were found in the Enamic for the ceramic component, these values are close to values reported for enamel at this size while the values for Lava Ultimate and Cerasmart were considerably lower than those of enamel (see Fig. 5). These observations rationalize the observations that enamel wear during abrasion was highest in the case of Enamic and much lower for Lava Ultimate and Cerasmart [17]. Regarding Enamic, the results differ slightly from a previous study that used nanoindentation to evaluate the properties of the two phases as well as the ceramic-polymer interface. In that study, the average elastic moduli of the ceramic, ceramic-polymer interface, and polymer phases were 62.68 ± 7.35, 47.78 ± 8.41, and 26.68 ± 7.31 GPa respectively [11].

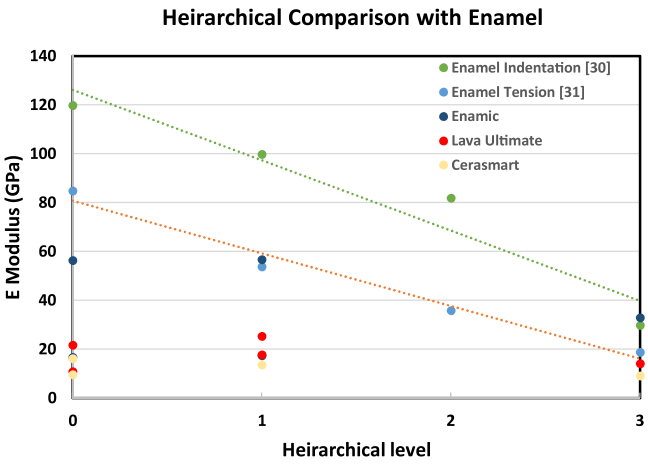

Fig. 5 – Comparison of the E modulus of the various CAD/CAM materials at the different size or hierarchical levels along with those of enamel. Trend lines have been added to the enamel tension and indentation derived values to enable better comparison with the CAD/CAM materials measured in this study.

4.3. *Nano level*

4.3.1. *Afm*

The determination of the elastic modulus using the AFM approach is relatively novel and there are relatively few studies that have undertaken such investigations [21,22,27]. The basis of the analysis has only been briefly described in the literature and the analysis procedure has been incorporated in the AFM's proprietary software. In addition, there appears to be no standardization procedure for ensuring the output from different or wearing tip geometries be incorporated. In the present approach, we originally assumed the tip geometry was as listed by the AFM tip supplier namely an 8 nm radius punch. The dilemma we faced was what parameters (punch or sphere and specific radius) be used to reprocess the results. Our approach is to use the complete histogram to generate an averaged $\hat{E}^*$ modulus and compare this with the E^* from the bulk macro data which assumes that the average E for the material is independent of specimen or scanned size, provided that the scan area is sufficiently larger than the microstructure. In addition, the actual E^* value is related to the depth of penetration, of the more realistic parabolic shape of the AFM tip, which is determined by the E modulus of the localized area of contact. Furthermore, the very sharp needle like form of the AFM tips, which although of pyramidal form have very acute angulation (<15°) especially when compared to a Berkovich indenter where the effective indenter angle is much greater at 70°.

The E modulus values for the ceramic, polymer phase of Enamic and the pre-reacted phase of the Lava Ultimate are in good agreement with the nano-indentation results, whereas the polymer matrix of the Lava Ultimate is significantly lower than the nano-indentation results. This may have arisen because of the limited size of the matrix phase, which may have resulted in the nanoindenter force-displacement response to be influenced by the surrounding stiffer pre-

reacted particles as the contact diameter is comparable to the width of the matrix phase. For Cerasmart, the AFM elastic modulus values fall either side of the nanoindenter results. There are stiffer particles present in this material that are typically 100–250 nm diameter that on close inspection appear to consist of broken pre-reacted ceramic-composite particles containing a nanofiller. This may explain the relatively low E value generated for this phase in the AFM results. It is also in keeping with the low E modulus as measured with the macro level and nanoindenter tests.

In this study, we have investigated the elastic modulus of CAD/CAM materials at three different levels to gain a deeper understanding of their potential clinical performance. However, it also should be stated that the lower E and H of these materials compared with other CAD/CAM ceramic (including glass-ceramics) and metal materials results in faster milling and polishing without additional thermal processing, which are very attractive features for chairside application. These materials have also been developed with the purpose of simulating the properties of enamel [7]. The hierarchical order of enamel according to Koenigswald and Clemen starts with the basic structural element of enamel, a single crystallite of hydroxyapatite, (level 0) which forms multiple crystallites (level 1). Bundles of these crystallites will form multiple prisms (level 2). The enamel type (level 3) is determined by the arrangement and orientation of the prisms. Finally, the overall distribution of different enamel types in a tooth is called "schmelzmuster" or enamel pattern (level 4) [28]. As stated by Ang et al. there have been relatively few studies that have explored the mechanical properties of enamel at the various hierarchical levels [29]. The latter authors used indentation with various sized indenter tips to determine "bulk enamel" (1–5 mm) which they defined as level 3, multiple rod $\tilde{5}0\,\mu m$ (defined as level 1) and single crystallites (10–50 nm) which they considered as level 0. Another study by Bechtle et al. measured the E modulus of enamel at various hierarchical scales using indentation to cause deflection of focused ion beam (FIB) milled cantilever beams of various sizes [30]. Tensile derived values of E at the various hierarchical levels by Bechtle et al. [30] were lower than the values derived in indentation induced compression by Ang et al. [29]. We are now in a position to relate our results of the different CAD/CAM materials at each dimensional scale to the values of elastic modulus at the different hierarchical levels of enamel (Fig. 5), except for level 2, as we didn't test the materials at a corresponding level. This comparison is important because the structural organization of enamel increase its tolerance to damage by toughening mechanisms associated with the hierarchy, which can be critical to achieve in a restorative material to impart equal durability to that of enamel [31]. These results show that enamel exhibits a substantial decline in its E modulus with dimension and that at the "bulk" level it is comparable to Enamic. At the smallest level, enamel consists of hydroxyapatite crystallites and proteins which have very high (120 GPa) and very low ($\tilde{1}$ GPa) values of E modulus. All of the ceramic-composite CAD/CAM materials evaluated had values of E of their constituents, over the scale levels measured, that were well below those of enamel with the exception of Enamic at the "bulk" level for tension and compression while Lava Ultimate was close to the enamel E modulus in tension. The size dependence of the elastic properties of enamel, as shown in Fig. 5, also raises issues with the use of nanoindentation E modulus data for numerical modelling of the stresses generated during the loading of teeth.

5. Conclusions

Based on the results of this *in-vitro* study, the following conclusions were drawn:

1 The ceramic-polymer CAD/CAM composite materials tested display E modulus values that are specimen size dependent. In all instances, the macro level values lay between the higher and lower values measured at the nano (AFM) level and to a lesser extent at the micro (nanoindenter) level. This outcome partially supports our hypothesis.
2 The values of E modulus at the various structural dimensions can be compared to enamel's elastic modulus values at similar hierarchical dimensions. At larger sizes, that is for a bulk tooth, the E modulus of Enamic is comparable to that measured for enamel while the Lava Ultimate has slightly inferior values to the tensile modulus of enamel.
3 Enamic is a stiffer material and shows minimal energy dissipation (low tan delta) during stressing even to a temperature of 180 °C. In contrast, Lava Ultimate and Cerasmart undergo limited plastic deformation under these conditions and show behavior indicative of a partially viscous material.

Acknowledgements

All materials were kindly donated by the manufacturers. The authors wish to acknowledge Kuwait University grant SRUL 01/14. M.V.S. acknowledges support of the Government of Russia through grant no. 14.Z50.31.0046.

REFERENCES

[1] Davidowitz G, Kotick P. The use of CAD/CAM in dentistry. Dent Clin North Am 2011;55:559–70.
[2] Mörmann W, Bindl A. All-ceramic, chair-side computer-aided design/computer-aided machining restorations. Dent Clin North Am 2002;46:405–26.
[3] Albakry M, Guazzato M, Swain MV. Effect of sandblasting, grinding, polishing and glazing on the flexural strength of two pressable all-ceramic dental materials. J Dent 2004;32:91–9.
[4] Cattell M, Clarke R, Lynch E. The transverse strength, reliability and microstructural features of four dental ceramics — part I. J Dent 1997;25:399–407.
[5] Ruse N, Sadoun M. Resin-composite blocks for dental CAD/CAM applications. J Dent Res 2014;93:1232–4.
[6] Lauvahutanon S, Takahashi H, Shiozawa M, Iwasaki N, Asakawa Y, Oki M, et al. Mechanical properties of composite resin blocks for CAD/CAM. Dent Mater J 2014;33(5):705–10.
[7] Mainjot AK, Dupont NM, Oudkerk JC, Dewael TY, Sadoun MJ. From artisanal to CAD-CAM blocks: state of the art of indirect composites. J Dent Res 2016;95:487–95.
[8] Coldea A, Swain M, Thiel N. Mechanical properties of polymer-infiltrated-ceramic-network materials. Dent Mater 2013;29:419–26.

[9] Coldea A, Swain M, Thiel N. In-vitro strength degradation of dental ceramics and novel PICN material by sharp indentation. J Mech Behav Biomed Mater 2013;26:34–42.
[10] Della Bona A, Corazza P, Zhang Y. Characterization of a polymer-infiltrated ceramic-network material. Dent Mater 2014;30:564–9.
[11] Awada A, Nathanson D. Mechanical properties of resin-ceramic CAD/CAM restorative materials. J Prosthet Dent 2015;114:587–93.
[12] Min J, Arola D, Yu D, et al. Comparison of human enamel and polymer-infiltrated-ceramic-network material "enamic" through micro- and nano-mechanical testing. Ceram Int 2016;42:10631–7.
[13] Bottino M, Campos F, Ramos N, et al. Inlays made from a hybrid material: adaptation and bond strengths. Oper Dent 2015;40:E83–91.
[14] Lawson N, Bansal R, Burgess J. Wear, strength, modulus and hardness of CAD/CAM restorative materials. Dent Mater 2016;32:e275–83.
[15] Albero A, Pascual A, Camps I, et al. Comparative characterization of a novel cad-cam polymer-infiltrated-ceramic-network. J Clin Exp Dent 2015;7:e495–500.
[16] He L, Swain M. A novel polymer infiltrated ceramic dental material. Dent Mater 2011;27:527–34.
[17] Mörmann W, Stawarczyk B, Ender A, et al. Wear characteristics of current aesthetic dental restorative CAD/CAM materials: two-body wear, gloss retention, roughness and Martens hardness. J Mech Behav Biomed Mater 2013;20:113–25.
[18] Stawarczyk B, Liebermann A, Eichberger M, et al. Evaluation of mechanical and optical behavior of current esthetic dental restorative CAD/CAM composites. J Mech Behav Biomed Mater 2016;55:1–11.
[19] Shigley JE. Mechanical engineering design. In: Budynas RG, Nisbett KJ, editors. Shigley's mechanical engineering design. New York: McGrow-Hill Primis; 2002. p. 44–184.
[20] Oliver W, Pharr G. Measurement of hardness and elastic modulus by instrumented indentation: advances in understanding and refinements to methodology. J Mater Res 2004;19:3–20.
[21] Haq S, Srivastava R. Measuring the influence of materials composition on nano scale roughness for wood plastic composites by AFM. Measurement 2016;30:541–7.
[22] Verbiest GJ, Rost MJ. Resonance frequencies of AFM cantilevers in contact with a surface. Ultramicroscopy 2016;31:70–6.
[23] Moore R. Intra-oral temperature variation over 24 hours. Eur J Orthod 1999;21:249–61.
[24] Mair L. Surface permeability and degradation of dental composites resulting from oral temperature changes. Dent Mater 1989;5:247–55.
[25] Béhin P, Stoclet G, Ruse N, et al. Dynamic mechanical analysis of high pressure polymerized urethane dimethacrylate. Dent Mater 2014;30:728–34.
[26] Shah PK, Stansbury JW, Bowman CN. Application of an addition–fragmentation-chain transfer monomer in di(meth)acrylate network formation to reduce polymerization shrinkage stress. Polym Chem 2017;8:4339–435.
[27] Lucas P, Philip S, Al-Qeoud D, et al. Structure and scale of the mechanics of mammalian dental enamel viewed from an evolutionary perspective. Evol Dev 2016;18:54–61.
[28] Koenigswald W, Clemens W. Levels of complexity in the microstructure of mammalian enamel and their application in studies of systematics. Scanning Microsc 1992;6:195–217.
[29] Ang SF, Bortel EL, Swain MV, Klocke A, Schneider GA. Size dependent elastic/inelastic behaviour of enamel over millimeter and nanometer length scales. Biomaterials 2010;31:1955–63.
[30] Bechtle S, Özcoban H, Lilleodden E, et al. Hierarchical flexural strength of enamel: transition from brittle to damage-tolerant behaviour. J R Soc Interface 2012;9:1265–74.
[31] Giannini M, Soares CJ, de Carvalho RM. Ultimate tensile strength of tooth structures. Dent Mater 2004;20:322–9.